

A Biophysically-Based Spectral Model of Light Interaction with Human Skin

Aravind Krishnaswamy and Gladimir V.G. Baranoski

Natural Phenomena Simulation Group, School of Computer Science, University of Waterloo, Ontario, Canada

Abstract

Despite the notable progress in physically-based rendering, there is still a long way to go before we can automatically generate predictable images of biological materials. In this paper, we address an open problem in this area, namely the spectral simulation of light interaction with human skin. We propose a novel biophysically-based model that accounts for all components of light propagation in skin tissues, namely surface reflectance, subsurface reflectance and transmittance, and the biological mechanisms of light absorption by pigments in these tissues. The model is controlled by biologically meaningful parameters, and its formulation, based on standard Monte Carlo techniques, enables its straightforward incorporation into realistic image synthesis frameworks. Besides its biophysically-based nature, the key difference between the proposed model and the existing skin models is its comprehensiveness, i.e., it computes both spectral (reflectance and transmittance) and scattering (bidirectional surface-scattering distribution function) quantities for skin specimens. In order to assess the predictability of our simulations, we evaluate their accuracy by comparing results from the model with actual skin measured data. We also present computer generated images to illustrate the flexibility of the proposed model with respect to variations in the biological input data, and its applicability not only in the predictive image synthesis of different skin tones, but also in the spectral simulation of medical conditions.

Categories and Subject Descriptors (according to ACM CCS): I.3.7 [Computer Graphics]: Three-Dimensional Graphics and Realism

1. Introduction

The modeling of light interaction with human skin is relevant in a variety of areas such as medicine, cosmetology and realistic image synthesis. By studying processes involved in light remission from skin through computer simulations, better protocols can be developed to automatically diagnose medical conditions, such as jaundice (yellowish hue), erythema (redness), as well as tumors at early stages [RKU*01, Tuc00]. Understanding how light is absorbed and propagated in skin tissues can assist in the design of lotions protective against harmful solar radiation, and also in the design of superior cosmetics. The games and entertainment industries can certainly benefit from being able to automatically generate realistic and predictable images of skin tissues. Creating images of human beings is usually an art left to designers and animators. Artists currently model skin by carefully adjusting rendering parameters such as textures

and colors. Despite its importance, the predictive rendering of organic materials, such as human skin, is still in its infancy, and many issues remain unsolved.

There is a considerable amount of research on skin optics available in the biomedical literature, as well as recent investigations in colorimetry. The models developed in these areas can be loosely classified into deterministic (e.g., applying Kubelka-Munk and diffusion theories [AP81]) and nondeterministic (e.g., applying Monte-Carlo methods [PKJW89]). A broad review of these models is beyond the scope of this work, and the interested reader is referred to more comprehensive texts on skin optics [KB04, Tuc00]. It is worth noting, however, that these models are mostly aimed at the reproduction of skin spectral properties to determine the content and distribution of various substances [ZBK01], i.e., scattering properties affecting skin appearance are usually not addressed. Moreover, a substantial portion of the

work done by the biomedical community is either laser-based or aimed at wavelengths outside the visible region of the light spectrum.

In computer graphics the focus has been on developing scattering models to be incorporated into image synthesis frameworks. Although the application requirements are somewhat different, algorithms and techniques used in the models mentioned above have been incorporated in computer graphics. In 1993, Hanrahan and Krueger [HK93] introduced to the graphics literature the algorithmic formulation for the simulation of tissue subsurface scattering proposed by biomedical researchers [PKJW89], which consists in applying Monte Carlo methods to simulate light transport in organic tissue. Ng and Li [NL01] extended the multilayer model proposed by Hanrahan and Krueger by adding a layer of oil on the outside of skin. Stam [Sta01] extended previous radiative transfer work based on discrete ordinate approximation in order to model a skin layer bounded by rough surfaces. Jensen *et al.* [JMLH01] proposed a model for simulating multiple scattering subsurface light transport in translucent materials, including human skin, which used a point source approximation based on the dipole method originally proposed by biomedical researchers. Although the computer graphics scattering models for human skin models are biologically motivated, they do not simulate important biological processes, such as the absorption of light by natural chromophores (pigments), which are closely tied with skin spectral properties. As a result, they must rely on spectral parameters (*e.g.*, reflectance and transmittance) either set by the user or obtained from the literature, which are specimen specific and usually limited to a narrow range of illuminating and viewing geometries.

Clearly, the predictive simulation of both the spectral and the spatial distribution of the light incident on human skin is still an open problem not only in graphics, but also in biomedicine and colorimetry. In this paper, we address this issue by proposing an algorithmic biophysically-based spectral model (henceforth referred to as BioSpec) specifically designed to account for the biological factors that affect light propagation and absorption in skin tissues. The BioSpec model is functionally comprehensive, *i.e.*, it takes as input biological and structural data and provides as output both spectral and scattering data for skin specimens. The former are provided in terms of reflectance and transmittance values, while the latter are given in terms of BSSDF (bidirectional surface-scattering distribution function), which can be decomposed into BRDF (bidirectional reflectance distribution function) and BTDF (bidirectional transmittance distribution function) components. The proposed model is controlled by biologically meaningful parameters determined through experiments described in the scientific literature, and its implementation, based on standard Monte Carlo Methods, enables its straightforward incorporation into most rendering frameworks. The spectral and scattering quantities

can be either computed and used on the fly during the rendering process or stored in a database to be used off-line.

The remainder of this paper is organized as follows. The next section describes the skin tissues and how they absorb and scatter light. Section 3 presents the algorithmic BioSpec model. Section 4 describes the approach used to evaluate the proposed model. Section 5 presents the results and discusses practical issues. Finally, Section 6 concludes the paper and outlines directions for future work.

2. Light Interaction with Human Skin

Skin is a multilayered and inhomogeneous organ (Figure 1). In this section, we outline the biological characteristics of its main constituents, and how they affect the propagation and absorption of light.

2.1. Structural Characteristics and Spectral Properties

The first and outermost section of human skin is the stratum corneum, which is a stratified structure approximately 0.01-0.02 mm thick [AP81, KB04]. There are skin structural models, however, that consider it part of another tissue, namely the epidermis [Tuc00]. The stratum corneum is composed mainly of dead cells, called corneocytes, embedded in a particular lipid matrix [TKK*01]. Light absorption is low in this tissue, with the amount of transmitted light being relatively uniform in the visible region of the light spectrum [EYSO66].

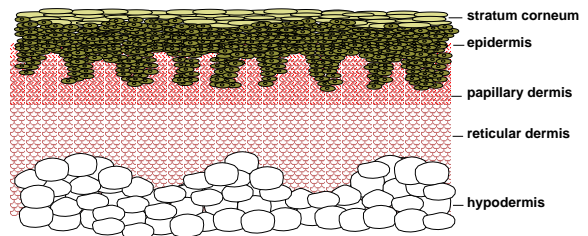


Figure 1: Schematic cross-section of human skin tissues and the subcutaneous fat tissue (hypodermis).

The epidermis is a 0.027-0.15mm thick structure [AP81, DT03, KB04] which propagates and absorbs light. The absorption property comes mostly from a natural chromophore, melanin. There are two types of melanin, the red/yellow pheomelanin and a brown/black eumelanin [THW*91]. Their absorption spectra are broad (Figure 2), with higher values for shorter wavelengths. The skin color is mostly associated with eumelanin [THW*91]. The ratio between the concentration of pheomelanin and eumelanin present in human skin varies from individual to individual, with much overlap between skin types [THW*91]. Recent studies reported values between 0.049 and 0.36 [PWK*03]. Melanin is produced by cells called melanocytes found in

membranous particles called melanosomes. The melanin absorption level depends on how many melanosomes per unit volume are in the epidermis. Typically, the volume fraction of the epidermis occupied by melanosomes varies from 1.3% (lightly pigmented specimens) to 43% (darkly pigmented specimens) [Jac96].

The dermis is a 0.6-3mm thick structure [AP81, DT03, KB04] which also propagates and absorbs light. It can be divided into two layers: the papillary dermis and the reticular dermis (Figure 1). These layers are primarily composed of dense, irregular connective tissue with nerves and blood vessels (smaller ones in the papillary, and larger ones in the reticular dermis). The volume fraction of blood in tissue can vary, roughly in the 0.2-7% range [Fle00, Jac96]. The fluence rate of blood decreases as we get deeper into the skin, following an almost linear pattern in the dermis [vGJSS89]. In the blood cells we find another natural chromophore, hemoglobin, which absorbs light and gives blood its reddish color. Normally, the hemoglobin concentration in whole blood is between 134 and 173g/L [YPR*02]. In the arteries, 90-95% of hemoglobin is oxygenated, and in the veins, more than 47% of the hemoglobin is oxygenated [Ang01]. These two types of hemoglobin, namely oxygenated and deoxygenated hemoglobin, have slightly different absorption spectra (Figure 2). Two other blood borne pigments are found in the dermis, bilirubin and β -carotene, which contribute to the yellowish or olive tint of human skin (Figure 2). We remark that β -carotene may be also found in the epidermis and stratum corneum [LMRPP75].

The hypodermis is a subcutaneous adipose tissue characterized by a negligible absorption of light in the visible region of the spectrum [Fle00]. It is usually not considered part of the skin, and its size varies considerably throughout the body. Due to the presence of white fat deposits, most of the visible light that reaches this tissue is reflected back to the upper layers [DT03].

2.2. Scattering Profile

The scattering profile of human skin has two main components: surface and subsurface scattering. Surface scattering follows Fresnel equations [SWXJ02], and it is affected by the presence of folds in the stratum corneum. The aspect ratio of these mesostructures depends on biological factors such as aging and hydration [TKK*01, TKL*02]. Approximately 5-7% of the light incident (over the entire spectrum) on the stratum corneum is reflected back to the environment [Tuc00]. The remaining portion is transmitted to the internal tissues. Besides the reflective-refractive scattering caused by the reflection and refraction of light at cellular boundaries, two other types of subsurface scattering occur within the skin layers: Mie and Rayleigh scattering [Jac96].

The stratum corneum and the epidermis are characterized

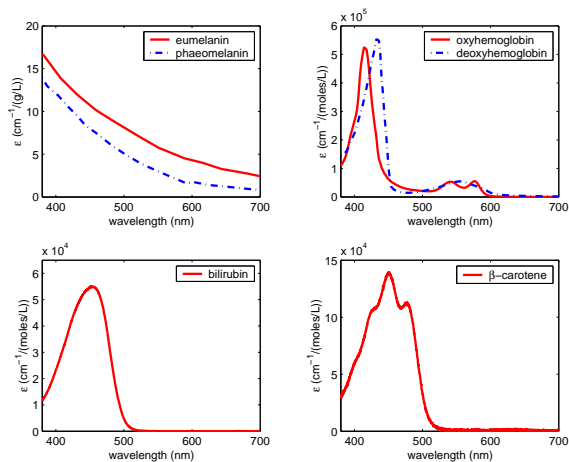


Figure 2: Spectral extinction coefficient curves for the natural pigments present in skin tissues. Courtesy of S. Prahl and the Oregon Medical Laser Center (OMLC).

as forward scattering media [BvdL84]. In the former this behavior is due to the alignment of the fibers, while in the latter it is due to Mie scattering caused by particles that are approximately the same size of the wavelength of light (e.g., cell organelles). The level of forward scattering for these tissues is wavelength dependent. Bruls and Leun [BvdL84] performed goniometric experiments for five wavelengths for both the stratum corneum and the epidermis, and they showed that the scattering profiles are broader towards the shorter wavelengths.

In the dermis, collagen fibers (approximately $2.8\mu\text{m}$ in diameter and cylindrical [Jac96]) are responsible for Mie scattering, while smaller scale collagen fibers (fibrils) and other micro-structures are responsible for Rayleigh scattering [Jac96]. Light gets scattered multiple times inside the dermis before it is either propagated to another layer or absorbed. This means that the spatial distribution of the light scattered within the dermis quickly becomes diffuse [AP81]. In fact, Jacques *et al.*, [JAP87] showed through goniometric measurements that backscattered light from the dermis is diffuse. While Mie scattering produces variations on both ends of the visible region of the light spectrum, Rayleigh scattering, being inversely proportional to the wavelength of light ($\approx \lambda^{-4}$), produces larger variations on the low end of the light spectrum [Jac96].

3. The BioSpec Model

In the BioSpec model, light propagation is described in terms of ray optics, and the wavelength of light, a physical optics parameter essential for biophysically-based rendering applications, is included by associating a wavelength with each ray. The propagation of light in the skin tissues is simulated as a random walk process [BR97], whose states are associated with the following interfaces:

1. air \Leftrightarrow stratum corneum;
2. stratum corneum \Leftrightarrow epidermis;
3. epidermis \Leftrightarrow papillary dermis;
4. papillary dermis \Leftrightarrow reticular dermis;
5. reticular dermis \Leftrightarrow hypodermis.

Once a ray hits the skin specimen at interface 1, it can be reflected back or refracted into the stratum corneum. From there, the ray can be reflected and refracted multiple times within the skin layers before it is either absorbed or propagated back to the environment thru interface 1. Recall that the hypodermis is a highly reflective medium (Section 2.2). Hence, for body areas characterized by the presence of this tissue, it is assumed total reflection at interface 5.

In the random walk implemented by the BioSpec model, the transition probabilities are associated with the Fresnel coefficients [BR97] computed at each interface (assuming that the cells are locally flat, *i.e.*, they are large with respect to the wavelength of the incoming light), and the termination probabilities are associated with the free path length (p) computed when a ray travels in the skin layers. The model takes into account the three components of a skin specimen's BSSDF: surface reflectance, subsurface reflectance and transmittance. These components are affected by the refractive indices differences at the interfaces, tissue scattering and absorption of light by skin pigments. In the next subsections, we describe how each of these components is simulated. Due to the stochastic nature of the simulations, we use several random numbers which are uniformly distributed in the interval $[0, 1]$ and represented by ξ_i for $i = 1..11$.

3.1. Reflection/Transmission at the Interfaces

The Fresnel equations [SWXJ02] indicate how much light is reflected and transmitted at a surface as a function of the angle of incidence (θ_i) and the refractive indices of the incidence and transmissive media. The refractive indices of the stratum corneum, epidermis, papillary dermis and reticular dermis are denoted by η_s , η_e , η_p and η_r respectively.

After computing the Fresnel coefficient (F) at an interface, we obtain a random number ξ_1 . If $\xi_1 \leq F$, then we generate a reflected ray, otherwise we generate a refracted ray. The reflected ray is computed applying the law of reflection, and the refracted ray is computed applying Snell's law [BR97].

3.2. Surface and Subsurface Scattering

A portion of the light that interacts with the stratum corneum cells is reflected back to the environment following the computation of the Fresnel coefficients described above. The spatial distribution of the reflected light varies according to the aspect ratio of the stratum corneum folds (Section 2.2). We represent these mesostructures as ellipsoids whose aspect ratio ($\sigma \in [0, 1]$) is defined as the quotient of the length

of the vertical axis by the length of the horizontal axis, which are parallel and perpendicular to the specimen's normal respectively. As the folds become flatter (lower σ), the reflected light becomes less diffuse. In order to account for this effect, we perturb the reflected rays using a warping function based on a surface-structure function proposed by Trowbridge and Reitz [TR75], which represents rough air-material interfaces using microareas randomly curved. This warping function [KB04] is given in terms of the polar (α_s) and azimuthal (β_s) perturbation angles as:

$$(\alpha_s, \beta_s) = \left(\arccos \left[\left(\frac{\sigma^2}{\sqrt{\sigma^4 - \sigma^4 \xi_2 + \xi_2}} - 1 \right)^{\frac{1}{2}} b \right], 2\pi \xi_3 \right) \quad (1)$$

where:

$$b = \frac{1}{\sigma^2 - 1}.$$

When a ray enters either the stratum corneum or the epidermis, it is scattered (Section 2.2). Scattering in either of these layers involves the perturbation of the incoming ray in both the polar (α_f) and azimuthal (β_f) angles. The scattering with respect to the azimuthal angle β_f is expected to be symmetric (equal in all directions) [PKJW89], thus we use $\beta_f = 2\xi_4\pi$. The scattering direction with respect to the polar angle α_f is computed using a randomized table look-up algorithm. Recall that Bruns and Leun [BvdL84] have performed goniometric measurements for stratum corneum and epidermis (Section 2.2). The polar scattering angles measured at a given wavelength by Bruns and Leun [BvdL84] are stored in a table, whose access indices correspond to the measured fractions of scattered radiation. For each ray we generate a random number ξ_5 , which we multiply by the table size. The integer part of the resulting value is used to access the corresponding polar scattering angle stored in the table. This spectral data oriented approach provides higher accuracy results than the use of data-fitting functions [BKK03].

Every ray entering one of the dermal layers is initially tested for Rayleigh scattering (Section 2.2). The Rayleigh scattering simulation performed by the BioSpec model combines atmospheric optics [McC76] and skin optics concepts [Jac96]. For the sake of conciseness, we present here only the key expressions used by the BioSpec model. The reader interested in their full derivation is referred to a technical report written by the authors [KB04].

In order to perform the Rayleigh test, we initially compute the spectral Rayleigh scattering amount (Equation 3), denoted by $R(\lambda)$, which is associated with the probability that the Rayleigh scattering can occur [McC76, KB04]. We then generate a random number ξ_8 . If $\xi_8 < 1 - \exp^{-R(\lambda)}$, then the ray is scattered using polar (α_R) and azimuthal (β_R) perturbation angles given by

$$(\alpha_R, \beta_R) = (\psi, 2\pi \xi_{10}) \quad (2)$$

where the angle ψ is obtained using rejection sampling in

conjunction with the Rayleigh phase function [KB04]:

$$\begin{aligned} &do \\ &\quad \psi = \pi \xi_9 \\ &\quad \chi = \frac{3}{2} \xi_{10} \\ &while \quad (\chi > \frac{3}{4} (1 + \cos^2 \psi)) \end{aligned}$$

According to Jacques [Jac96], collagen fibers occupy 21% of the dermal volume, and the Rayleigh scattering in this tissue can be approximated using spheres mimicing the ultrastructure associated with the random arrays of collagen fibrils of radius r . This results in a fiber density given by $N = 0.21 (\frac{4}{3} r^3 \pi)^{-1}$, which one can use to compute the spectral Rayleigh scattering amount through the following equation:

$$R(\lambda) = \frac{8\pi^3 ((\frac{\eta_f}{\eta_m})^2 - 1)^2}{3N\lambda^4} \left(\frac{t}{\cos \theta} \right) \quad (3)$$

where:

- η_f = index of refraction of the fibers,
- η_m = index of refraction of the dermal medium,
- t = thickness of the medium,
- θ = angle ($< 90^\circ$) between the ray direction and the specimen's normal direction.

Recall that light becomes diffuse in the dermis (Section 2.2). Hence, if the Rayleigh test fails or the ray has already been bounced off one of the dermal interfaces, then the ray is randomized around the normal direction using a warping function based on a cosine distribution [BR97]. This warping function is given in terms of the polar (α_d) and azimuthal (β_d) perturbation angles as:

$$(\alpha_d, \beta_d) = (\arccos(\sqrt{\xi_6}), 2\pi\xi_7) \quad (4)$$

3.3. Absorption

When a ray travels in a given layer, it is first scattered as described in the previous section. The ray is then tested for absorption. If the ray is not absorbed, then it is propagated to the next layer. The absorption testing done by the BioSpec model is based on Beer's law [BR97, Tuc00]. It is performed probabilistically every time a ray starts a run in a given layer. It consists of estimating the ray free path length (p) through the following expression:

$$p(\lambda) = -\frac{1}{a_i(\lambda)} \ln(\xi_{11}) \cos \theta \quad (5)$$

where:

- $a_i(\lambda)$ = total absorption coefficient of pigments of given layer i ,
- θ = angle between the ray direction and the specimen's normal direction.

If $p(\lambda)$ is greater than the thickness of the pigmented medium (both expressed in cm), then the ray is propagated, otherwise it is absorbed. In the BioSpec formulation the

thickness of the stratum corneum, epidermis, papillary dermis and reticular dermis are denoted by t_s , t_e , t_p and t_r respectively.

The BioSpec model accounts for the presence of eumelanin, pheomelanin, oxyhemoglobin, deoxyhemoglobin, bilirubin and β -carotene. The spectral extinction coefficients for these pigments, denoted $\epsilon_{eu}(\lambda)$, $\epsilon_{ph}(\lambda)$, $\epsilon_{ohb}(\lambda)$, $\epsilon_{dhb}(\lambda)$, $\epsilon_{bil}(\lambda)$ and $\epsilon_{car}(\lambda)$ respectively, are obtained from the curves shown in Figure 2. The total absorption coefficient for each layer is simply the sum of the absorption coefficient for each pigment present in the layer, which is obtained by multiplying the pigment's spectral extinction coefficient by its estimated concentration in the layer.

It is difficult to accurately determine the baseline absorption coefficient for pigmentless skin tissues. Furthermore, due to its low magnitude compared to the absorption coefficients of the skin chromophores [Sai94], skin optics researchers usually assume that its effects are negligible [Ang01]. For the sake of completeness, however, we include the baseline skin absorption coefficient ($a_{base}(\lambda)$) in the absorption equations.

The stratum corneum total absorption coefficient is given by:

$$a_1(\lambda) = a_{base}(\lambda) + a_{cs}(\lambda) \quad (6)$$

where:

- $a_{cs}(\lambda)$ = β -carotene absorption coefficient.

The absorption coefficient a_{cs} is given by:

$$a_{cs}(\lambda) = \frac{\epsilon_{car}(\lambda)}{537} c_{cs} \quad (7)$$

where:

- 537 = molecular weight of beta-carotene ($g/mole$),
- c_{cs} = β -carotene concentration in the stratum corneum ($\frac{g}{L}$).

The epidermis total absorption coefficient is given by:

$$\begin{aligned} a_2(\lambda) = & (a_{eu}(\lambda) + a_{ph}(\lambda)) \vartheta_m \\ & + (a_{base}(\lambda) + a_{ce}(\lambda))(1 - \vartheta_m) \end{aligned} \quad (8)$$

where:

- $a_{eu}(\lambda)$ = eumelanin absorption coefficient,
- $a_{ph}(\lambda)$ = pheomelanin absorption coefficient,
- $a_{ce}(\lambda)$ = β -carotene absorption coefficient in the epidermis,
- ϑ_m = volume fraction (%) of the epidermis occupied by melanosomes $\div 100$.

The absorption coefficient for eumelanin is given by:

$$a_{eu}(\lambda) = \epsilon_{eu}(\lambda) c_{eu} \quad (9)$$

where:

- c_{eu} = eumelanin concentration ($\frac{g}{L}$).

Similarly, the absorption coefficient for pheomelanin ($a_{ph}(\lambda)$) is computed by multiplying its spectral extinction

coefficient ($\epsilon_{ph}(\lambda)$) by its concentration (c_{ph}). Also, the absorption coefficient a_{ce} is obtained by replacing c_{cs} by the concentration of β -carotene (c_{ce}) in Equation 7.

The papillary dermis total absorption coefficient is given by:

$$a_3 = (a_{ohb}(\lambda) + a_{dhb}(\lambda) + a_{cd}(\lambda) + a_{bil}(\lambda)) \vartheta_p + a_{base}(\lambda)(1 - \vartheta_p) \quad (10)$$

where:

- $a_{ohb}(\lambda)$ = oxyhemoglobin absorption coefficient,
- $a_{dhb}(\lambda)$ = deoxyhemoglobin absorption coefficient,
- $a_{cd}(\lambda)$ = β -carotene absorption coefficient in the dermal layers,
- $a_{bil}(\lambda)$ = bilirubin absorption coefficient,
- ϑ_p = volume fraction (%) of the papillary dermis occupied by whole blood $\div 100$.

The absorption coefficient a_{cd} is obtained by replacing c_{cs} by the concentration of β -carotene in the dermal layers (c_{cd}) in Equation 7. Also, recall that the volume fractions of blood vary within the dermis tissue (Section 2.1). Hence, to compute the reticular dermis total absorption coefficient (a_4), we replace ϑ_p by ϑ_r (volume fraction (%) of the reticular dermis occupied by whole blood $\div 100$) in Equation 10.

The absorption coefficient for oxyhemoglobin is given by:

$$a_{ohb}(\lambda) = \frac{\epsilon_{ohb}(\lambda)}{66500} c_{hb} * \gamma \quad (11)$$

where:

- 66500 = molecular weight of hemoglobin ($g/mole$),
- c_{hb} = concentration of hemoglobin in the blood ($\frac{g}{L}$),
- γ = ratio of oxyhemoglobin to the total hemoglobin concentration.

Similarly, the absorption coefficient for deoxyhemoglobin ($a_{dhb}(\lambda)$) is computed using its spectral extinction coefficient ($\epsilon_{dhb}(\lambda)$) and replacing γ by $(1 - \gamma)$ in Equation 11.

Finally, the absorption coefficient of bilirubin is given by:

$$a_{bil}(\lambda) = \frac{\epsilon_{bil}(\lambda)}{585} c_{bil} \quad (12)$$

where:

- 585 = molecular weight of bilirubin ($g/mole$),
- c_{bil} = bilirubin concentration ($\frac{g}{L}$).

4. Evaluation Issues

Usually models of light interaction with matter are evaluated by visually inspecting the images generated using such models. Clearly, such an evaluation may be biased by factors not directly related to the model. For example, a careful modeling of skin's geometrical details [HGE01, TKL*02] and an accurate post-processing tone reproduction [GAL*97] may improve the realistic appearance of skin specimens. These aspects, however, are addressed in other important areas of research, and they are beyond the scope of this work.

A current trend is to perform comparisons between model readings and measured data so that the models can be used in a predictive manner [GAL*97]. We used this approach in this work, *i.e.*, the BioSpec model was tested as a separated unit of the rendering pipeline and the results were compared with actual measured data [EYSO66, MWL*99, VGI94]. These comparisons were performed using a virtual spectrophotometer and a virtual goniophotometer [BR97], and reproducing the actual measurement conditions as faithfully as possible. The biophysical input data used in our experiments, unless otherwise stated in the text, is presented in Table 1. The computer generated images presented in the next section serve two purposes. First, to illustrate the applicability of the BioSpec model in the spectral simulation of medical conditions associated with changes in the biophysical parameters. Second, to highlight an aspect for which measured data is scarce, namely the translucency of skin tissues. These images were rendered using a standard Monte Carlo path-tracing algorithm.

Parameter	Default Value	Source
r	25nm	[Li03]
η_s	1.55	[AP81]
η_e	1.4	[Tuc00]
η_p	1.36	[JAP87]
η_r	1.38	[JAP87]
η_f	1.5	[Jac96]
t_s	0.001cm	[AP81]
t_e	0.01cm	[AP81]
t_p	0.02cm	[AP81]
t_r	0.18cm	[AP81]
c_{eu}	80g/L	[THW*91]
c_{ph}	12g/L	[THW*91]
c_{cs}	$2.1^{-4}g/L$	[LMRPP75]
c_{ce}	$2.1^{-4}g/L$	[LMRPP75]
c_{cd}	$7.0^{-5}g/L$	[LMRPP75]
c_{hb}	150g/L	[Fle00]
c_{bil}	0.05g/L	[RKU*01]
ϑ_m	5.2%	[Jac96]
ϑ_p	1.2%	[Ang01]
ϑ_r	0.91%	[Ang01]
γ	75%	[Ang01]
σ	0.75	[TKK*01, TKL*02]

Table 1: Data used in the evaluation of the BioSpec model.

5. Results and Discussion

Figure 3 presents comparisons of modeled reflectance curves provided by the BioSpec model with actual measured curves provided by Vrhel *et al.* [VGI94] (available in the North Carolina State University (NCSU) spectra database) for lightly and moderately pigmented specimens. The measurements

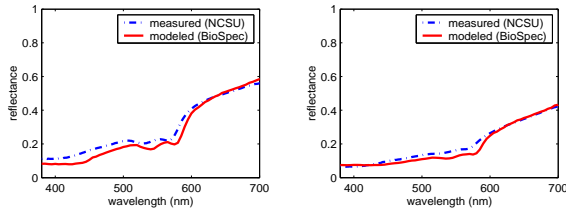


Figure 3: Comparison of modeled reflectance curves provided by the BioSpec model with actual measured curves available in the NCSU spectra database [VGI94]. Left: lightly pigmented skin specimen (NCSU file 113). Right: moderately pigmented specimen (NCSU file 82).

were performed considering $\theta_i = 45^\circ$ [VGI94]. We can observe that the reflectance curves provided by the BioSpec model are qualitatively in agreement with the actual measured curves. The quantitative discrepancies may be due in part to the fact that some parameters used in our simulations have to be estimated based on the overall description of the specimens (e.g., in these experiments we set $\vartheta_m = 5.2\%$ and $\vartheta_m = 10\%$ for the lightly and moderately pigmented specimens respectively [Jac96]) and other parameters correspond to average values found in the literature (e.g., the refractive indices for the skin layers). Furthermore, the exact position of the absorption peaks of natural pigments depends on the solvents in which they are dissolved, and one can expect small shifts when comparing to *in vivo* values [SR85].

The measured transmittance data for human skin available in the scientific literature, to the best of our knowledge, is limited to separated skin layers. Figure 4 presented comparisons between modeled and actual measured transmittance curves for the stratum corneum and epidermis tissues of two specimens, a moderately and a heavily pigmented one. The measured curves were provided by Everett *et al.* [EYSO66], and they were obtained at a normal angle of incidence ($\theta_i = 0^\circ$). Everett *et al.* [EYSO66] reported thickness values for the moderately pigmented ($t_s = 0.0017\text{cm}$ and $t_e = 0.0025\text{cm}$) and the heavily pigmented ($t_s = 0.0023\text{cm}$ and $t_e = 0.0021\text{cm}$) specimens. Based on their description of the specimens, we set $\vartheta_m = 9.5\%$ and $\vartheta_m = 38\%$ for the lightly and heavily specimens respectively. Again, we can observe a qualitative agreement between the modeled and the actual measured curves. The quantitative discrepancies, also related to the factors mentioned above, are noticeable but within acceptable accuracy boundaries since the measured curves have a reported tolerance of $\approx \pm 5\%$ [EYSO66].

The overall reflectance of human skin presents interesting features. As expected, darker skin (characterized by higher volume fractions of epidermis occupied by melanosomes) reflects less light than lighter skin. However, lightly pigmented skin presents a characteristic “W” shape in the reflectance curves between 500nm and 600nm [Ang01]. Oxygenated hemoglobin is responsible for this feature, which

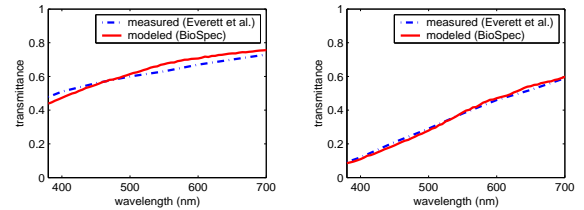


Figure 4: Comparison of modeled transmittance curves (for the stratum corneum and epidermis tissues) provided by the BioSpec model with actual measured curves provided by Everett *et al.* [EYSO66]. Left: moderately pigmented specimen. Right: heavily specimen.

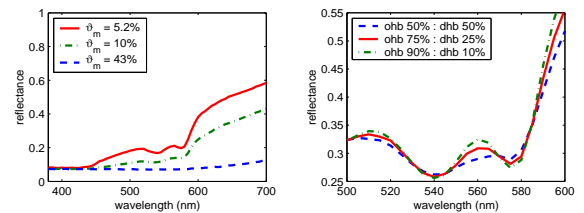


Figure 5: Comparison of modeled spectral curves provided by the BioSpec model ($\theta_i = 45^\circ$) considering the variation of biological parameters. Left: volume fractions of epidermis occupied by melanosomes (ϑ_m). Right: ratio of oxygenated (ohb) to deoxygenated (dhb) hemoglobin in the dermal layers.

can be accentuated as the proportion of oxyhemoglobin with respect to total hemoglobin increases [ZBK01]. The graphs presented in Figure 5 indicate that the BioSpec model can capture these optical characteristics of human skin.

Figure 6 shows a comparison between modeled and actual measured skin BRDFs provided by Marschner *et al.* [MWL*99]. Since the BioSpec model provides spectral readings, we needed to integrate spectral values over the visible region of the light spectrum in order to obtain data that could be compared to the data provided by Marschner *et al.* [MWL*99]. Based on the lightly pigmented specimen’s description provided by Marschner *et al.* [MWL*99], we set $\vartheta_m = 2.5\%$ in these experiments. As illustrated by the measurements provided by Marschner *et al.* [MWL*99] (Figure 6 (left)), the BRDF of skin specimens presents an angular dependence, and it becomes more diffuse for small angles. Figure 6 (right) shows that the BioSpec model can represent this angular dependency, and the modeled BRDF curves generally agree with the measured BRDF curves provided by Marschner *et al.* [MWL*99]. The most noticeable quantitative discrepancies are observed for the larger angle of incidence, namely $\theta_i = 60^\circ$. It is worth noting, however, that besides the previously mentioned factors that quantitatively affect the modeled curves, one should also consider the sources of noise in the measurements performed by Marschner *et al.* [MWL*99], which include deviations in

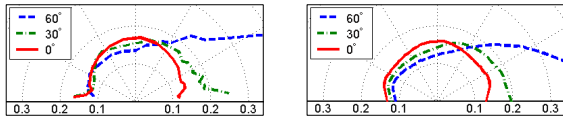


Figure 6: Comparison of BRDF curves for a lightly pigmented specimen. Left: actual measured BRDF curves provided by Marschner et al. [MWL*99]. Right: modeled BRDF curves provided by the BioSpec model.

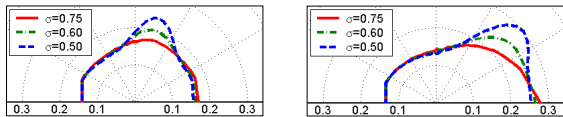


Figure 7: Comparison of modeled spectral curves provided by the BioSpec model considering variations on the aspect ratio (σ) of the stratum corneum folds. Left: $\theta_i = 15^\circ$. Right: $\theta_i = 45^\circ$.

the specimen's normal estimation and spatial variations in the measured BRDFs.

Skin specimens characterized by thin and numerous folds (e.g., young and/or hydrated specimens) present a directional behavior stronger than specimens with wider but fewer folds (e.g., old and/or dry specimens) [MWL*99, TKK*01, TKL*02]. The former case corresponds to folds with lower aspect ratio, while the latter case corresponds to folds with a higher aspect ratio [TKK*01, TKL*02]. Figure 7 presents modeled BRDF curves for two angles of incidence, namely $\theta_i = 15^\circ$ and $\theta_i = 45^\circ$, obtained by varying the parameter σ associated with the folds' aspect ratio. These curves show that the BioSpec model can qualitatively simulate the variation in the scattering behavior of skin specimens associated with changes in the aspect ratio of the stratum corneum folds.

A mechanical, chemical, electrical, thermal or luminous stimulus can induce a reddening around the stimulation site on the skin. This abnormal redness of the skin, which may be also due to an inflammation [Tuc00], is caused by a dilation of the blood vessels followed by an increase in the volume fractions of blood in the dermal layers. Figure 8 shows images generated to illustrate the capability of the BioSpec model of spectrally simulate this medical condition by varying, within actual biological limits, the parameters associated with the increase of the volume fractions of blood in the papillary (ϑ_p) and reticular (ϑ_r) dermis.

Jaundice, or hyperbilirubinemia [RKU*01, Sai94], is a medical symptom associated with the accumulation of bilirubin in the dermal tissues. It is usually caused by liver or gall bladder disorders, and it is characterized by the yellowish appearance of the skin and eyes. Figure 9 shows images generated to illustrate the capability of the BioSpec model of spectrally simulate this medical symptom by varying, within actual biological limits, the parameters associated with the



Figure 8: Images generated using the BioSpec model to spectrally simulate erythema conditions. Left: $\vartheta_p = 1.2\%$ and $\vartheta_r = 0.91\%$. Center: $\vartheta_p = 2.7\%$ and $\vartheta_r = 0.3\%$. Right: $\vartheta_p = 3.6\%$ and $\vartheta_r = 0.4\%$.



Figure 9: Images generated using the BioSpec model to spectrally simulate jaundice symptoms. Left: $c_{bil} = 0.05\text{g/L}$. Center: $c_{bil} = 0.5\text{g/L}$. Right: $c_{bil} = 3.0\text{g/L}$.

increase of bilirubin concentration (c_{bil}) in the dermal layers.

The BTDF of the whole skin can be observed (*in vivo*) in body parts with a thin or absent hypodermis, such as ears, eye lids and fingers. In these areas the behavior of the transmitted light is near Lambertian, to the point where no internal structure can be noticeable [RYY*02]. Figure 10 presents images generated using the BioSpec model to illustrate the translucency of skin tissues as well as its variations due to different melanin pigmentation levels.

6. Conclusion and Future Work

We presented a novel biophysically-based model for light interaction with human skin. It provides both spectral and scattering data for skin specimens, and it is controlled by biologically meaningful parameters. Results from the model were compared with results from actual experiments. These comparisons showed good agreement between modeled and measured data, and strengthened our confidence in the predictability of the proposed model. They also suggested that there is still room for improvement.

As future work, from a scattering point of view, we intend to investigate factors affecting the anisotropy of skin specimens, such as the presence of wrinkles. External factors, such as cosmetics, oil and sweat, may affect the skin's BRDF and light polarization. These factors will be examined in the next stage of our research as well. From a spectral point of view, we plan to extend the model's scope to the ultraviolet and infrared regions of the light spectrum and incorporate time dependent mechanisms of photon reemission.

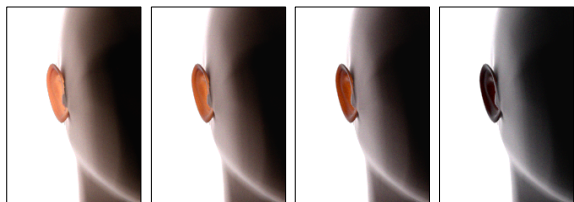


Figure 10: Images generated using the BioSpec model to show variations in the translucency of skin tissues associated with different levels of melanin pigmentation. From left to right: $\vartheta_m = 1.9\%$, $\vartheta_m = 5.2\%$, $\vartheta_m = 12\%$ and $\vartheta_m = 42\%$.

These features would allow us to use the proposed model in the visual simulation of biological processes affecting both the appearance and health of human skin, such as fluorescence and tanning, as well as the formation of melanomas.

Acknowledgements

The authors would like to thank Michael Lam for his helpful suggestions on the Rayleigh scattering simulation, and Inscrubber Technology Corporation for equipment use. The work presented in this paper was supported by the Natural Sciences and Engineering Research Council of Canada (NSERC grant 238337) and the Canada Foundation for Innovation (CFI grant 33418).

References

- [Ang01] ANGELOPOULOU E.: Understanding the color of human skin. In *Human Vision and Electronic Imaging VI* (2001), SPIE, vol. 4299, pp. 243–251.
- [AP81] ANDERSON R., PARRISH J.: The optics of human skin. *Journal of Investigative Dermatology* 77, 1 (1981), 13–19.
- [BKK03] BARANOSKI G., KRISHNASWAMY A., KIMMEL B.: *Revisiting the Foundations of Sub-surface Scattering*. Tech. Rep. CS-2003-45, School of Computer Science, University of Waterloo, Canada, December 2003.
- [BR97] BARANOSKI G., ROKNE J.: An algorithmic reflectance and transmittance model for plant tissue. *Computer Graphics Forum (EUROGRAPHICS Proceedings)* 16, 3 (September 1997), 141–150.
- [BvdL84] BRULS W., VAN DER LEUN J.: Forward scattering properties of human epidermal layers. *Photochem. Photobiol.* 40 (1984), 231–242.
- [DT03] DOI M., TOMINAGA S.: Spectral estimation of human skin color using the Kubelka-Munk theory. In *SPIE/IS&T Electronic Imaging* (2003), SPIE, vol. 5008, pp. 221–228.
- [EYSO66] EVERETT M., YEARGERS E., SAYRE R., OLSEN R.: Penetration of epidermis by ultraviolet rays. *Photochemistry and Photobiology* 5 (1966), 533–542.
- [Fle00] FLEWELLING R.: Noninvasive optical monitoring. In *The Biomedical Engineering Handbook* (Boca Raton, USA, 2000), Bronzino J., (Ed.), IEEE Press, pp. 1–11. Section 86.
- [GAL*97] GREENBERG D., ARVO J., LAFORTUNE E., TORRANCE K., FERWERDA J., WALTER B., TRUMBORE B., SHIRLEY P., PATTANAIK S., FOO S.: A framework for realistic image synthesis. In *SIGGRAPH, Annual Conference Series* (1997), pp. 477–494.
- [HGE01] HARO A., GUENTER B., ESSA I.: Real-time, photo-realistic, physically based rendering of fine scale human skin structure. In *Rendering Techniques'2001 (Proceedings of the 12th Eurographics Rendering Workshop)* (London, June 2001), Hanrahan P. M., Purgathofer W., (Eds.), Springer-Verlag, pp. 53–62.
- [HK93] HANRAHAN P., KRUEGER W.: Reflection from layered surfaces due to subsurface scattering. In *SIGGRAPH, Annual Conference Series* (August 1993), pp. 165–174.
- [Jac96] JACQUES S.: Origins of tissue optical properties in the uva visible and nir regions. *OSA TOPS on Advances in Optical Imaging and Photon Migration 2* (1996), 364–369.
- [JAP87] JACQUES S., ALTER C., PRAHL S.: Angular dependence of HeNe laser light scattering by human dermis. *Lasers in Life Sciences* 1, 4 (1987), 309–333.
- [JMLH01] JENSEN H., MARSCHNER S., LEVOY M., HANRAHAN P.: A practical model for subsurface light transport. In *SIGGRAPH, Annual Conference Series* (August 2001), pp. 511–518.
- [KB04] KRISHNASWAMY A., BARANOSKI G.: *A Study on Skin Optics*. Tech. Rep. CS-2004-01, School of Computer Science, University of Waterloo, Canada, January 2004.
- [Li03] LI S.: Biologic biomaterials: Tissue-derived biomaterials (collagen). In *Biomaterials Principles and Applications* (Boca Raton, USA, 2003), Park J., Bronzino J., (Eds.), CRC Press, pp. 117–139.
- [LMRPP75] LEE R., MATHEWS-ROTH M., PATHAK M., PARRISH J.: The detection of carotenoid pigments in human skin. *Journal of Investigative Dermatology* 64 (1975), 175–177.

- [McC76] MCCARTNEY E.: *Optics of the Atmosphere: Scattering by Molecules and Particles*. John Wiley & Sons Inc., 1976.
- [MWL*99] MARSCHNER S., WESTIN S. H., LAFORTUNE E., TORRANCE K., GREENBERG D.: Image-based brdf measurement including human skin. In *Rendering Techniques'1999 (Proceedings of the 10th Eurographics Rendering Workshop)* (Granada, June 1999), Lischinski D., Larson G. W., (Eds.), Springer-Verlag, pp. 119–130.
- [NL01] NG C., LI L.: A multi-layered reflection model of natural human skin. In *Computer Graphics International 2001* (Hong Kong, July 2001), pp. 249–256.
- [PKJW89] PRAHL S., KEIJZER M., JACQUES S., WELCH A.: A Monte Carlo model of light propagation in tissue. *SPIE Institute Series IS 5* (1989), 102–111.
- [PWK*03] PARSAD D., WAKAMATSU K., KANWAR A., KUMAR B., ITO S.: Eumelanin and pheomelanin contents of depigmented and repigmented skin in vitiligo patients. *British Journal of Dermatology 149* (2003), 624–626.
- [RKU*01] ROLINSKY B., KÜSTER H., UGELE B., GRUBER R., HORN K.: Total bilirubin measurement by photometry on a blood gas analyser: potential for use in neonatal testing at point of care. *Clinical Chemistry 47*, 10 (2001), 1845–1847.
- [RYY*02] RODRIGUEZ J., YAROSLAVSKY I., YAROSLAVSKY A., BATTARBEE H., TUCHIN V.: Time-resolved imaging in diffusive media. In *Handbook of Optical Biomedical Diagnostics* (Bellingham, WA, USA, 2002), Tuchin V., (Ed.), SPIE Press, pp. 357–404.
- [Sai94] SAIDI I.: *Transcutaneous optical measurement of hyperbilirubinemia in neonates*. PhD thesis, Rice University, USA, 1994.
- [SR85] SALISBURY F., ROSS C.: *Plant Physiology*, third ed. Wadsworth Publishing Company, Belmont, California, 1985.
- [Sta01] STAM J.: An illumination model for a skin layer bounded by rough surfaces. In *Rendering Techniques'2001 (Proceedings of the 12th Eurographics Rendering Workshop)* (London, June 2001), Hanrahan P. M., Purgathofer W., (Eds.), Springer-Verlag, pp. 39–52.
- [SWXJ02] SU Y., WANG W., XU K., JIANG C.: The optical properties of skin. In *Optics in Health Care and Biomedical Optics: Diagnostics and Treatment* (2002), SPIE, vol. 4916, pp. 299–304.
- [THW*91] THODY A., HIGGINS E., WAKAMATSU K., ITO S., BURCHILL S., MARKS J.: Pheomelanin as well as eumelanin is present in human dermis. *Journal of Investigative Dermatology 97* (1991), 340–344.
- [TKK*01] TALREJA P., KASTING G., KLEENE N., PICKENS W., WANG T.: Visualization of the lipid barrier and measurement of lipid path-length in human stratum corneum. *AAPS PharmSci 3*, 2 (2001), 1–9.
- [TKL*02] THALMANN N., KALRA P., LÉVÊQUE J., BAZIN R., BATISSE D., QUERLEUX B.: A computational skin model: fold and wrinkle formation. *IEEE Transactions on Information Technology in Biomedicine 6*, 4 (2002), 317–323.
- [TR75] TROWBRIDGE T., REITZ K.: Average irregularity representation of a rough surface for ray reflection. *Journal of the Optical Society of America 65*, 5 (May 1975), 531–536.
- [Tuc00] TUCHIN V.: *Tissue Optics Light Scattering Methods and Instruments for Medical Diagnosis*. The International Society for Optical Engineering, Bellingham, WA, USA, 2000.
- [VGI94] VRHEL M., GERSHON R., IWAN L.: Measurement and analysis of object reflectance spectra. *Color Research and Application 19*, 1 (1994), 4–9.
- [vGJSS89] VAN GEMERT M., JACQUES S., STERENBORG H., STAR W.: Skin optics. *IEEE Transactions on Biomedical Engineering 36*, 12 (1989), 1146–1154.
- [YPR*02] YAROSLAVSKY A., PRIEZZHEV A., RODRIGUEZ J., YAROSLAVSKY I., BATTARBEE H.: Optics of blood. In *Handbook of Optical Biomedical Diagnostics* (Bellingham, WA, USA, 2002), Tuchin V., (Ed.), SPIE Press, pp. 169–216.
- [ZBK01] ZONIOS G., BYKOWSKY J., KOLLIAS N.: Skin melanin, hemoglobin, and light scattering properties can be quantitatively assessed in vivo using diffuse reflectance spectroscopy. *Journal of Investigative Dermatology 117*, 6 (2001), 1452–1457.